Optimization of LaNi5 hydrogen storage properties by the combination of mechanical alloying and element substitution

Yuchen Liu[a,b], Djafar Chabane[a,b], Omar Elkedim[a,b]

a. FEMTO-ST Institute, Univ. Bourgogne Franche-Comte, UTBM, CNRS, Belfort, France
b. FCLAB, Univ. Bourgogne Franche-Comte, CNRS, Belfort, France
Corresponding author : Yuchen Liu
Email adresse : yuchen.liu@utbm.fr
Telephone : +33 749828826

Abstract

$LaNi_5$ is a commercial hydrogen storage alloy with great potential. But its performance still needs to be optimized to meet the standard proposed by the US Department of Energy. Element substitution is a very important method to optimize the performance of hydrogen storage alloys, especially suitable for AB_5 alloys. As a novel method to produce nanocrystalline hydrogen storage alloys, mechanical alloying is also often applied to optimize the properties of hydrogen storage alloys.

In this work, first of all, the simulation method based on first principles is applied to predict the performance of 8 elements substituting Ni respectively, and select the most suitable element to substitute Ni. Then the phase composition characterization and hydrogen storage performance test were carried out. It was found that mechanical alloying can greatly improve the hydrogen storage performance of $LaNi_5$, and different ball milling times can bring about different performance changes. After adding Cr to the ball-milled $LaNi_5$, the properties of the formed $LaNi_4Cr$ were further improved.

Key word: Hydrogen storage alloys; $LaNi_5$ optimization; Total energy; Mechanical alloying; Electrochemical tests

1.Introduction

Solid-state hydrogen storage is a promising hydrogen storage method [1-3]. Among various hydrogen storage materials, hydrogen storage alloys store hydrogen in the form of atoms into the alloy to form hydrides. This method not only has high theoretical capacity, but also is safe, low in cost, and easy to transport and store [4-6]. A large number of alloys have been studied whether they can be used for hydrogen storage. Among them, rare earth-based alloys have been found to be an excellent hydrogen storage alloy because of their good hydrogen storage capacity, good kinetics and cycle stability [7-9]. The chemical formula of rare earth-based hydrogen

storage alloy is AB_n (n=1, 2, 3, 5...), A is a rare earth metal, B is a post-transition metal [10]. Among rare earth-based alloys, $LaNi_5$ has been used as a commercial hydrogen storage alloy for anodes in Ni-MH batteries because of its high volumetric energy density and mild operating conditions [11][12]. However, although its performance is excellent, it is still difficult to meet the standards proposed by the US Department of Energy [13].

Researchers have proposed numerous approaches to optimize the performance of $LaNi_5$. Joubert et al. [14] summarize the current status and performance optimization of AB_5 alloys. They believe that although the structure of $LaNi_5$ is simple, it can reversibly store a large amount of hydrogen, and can also accommodate a large number of substituting elements, so that the properties of the compound can be changed to a large extent as needed. As mentioned above, element substitution is the best way to improve the hydrogen storage performance of $LaNi_5$. Todorova et al [15] studied the effect of Al replacing Ni on the hydrogen storage properties of $LaNi_5$. He found that for $LaNi_{5-x}Al_x$ alloys, at higher aluminum concentrations ($0.1 < x < 1.0$), the hydrogen storage capacity decreased significantly with the increase of aluminum addition, and the electrochemical charging / discharge also follows this rule. Somo et al. [16] investigated the hydrogen storage properties of $LaNi_{5-x}Sn_x$ (X = 0.2) alloys using Sn substituting Ni and depositing Pd on the surface. The results show that substituting a small portion of Sn for Ni can increase the hydrogen absorption capacity of the alloy, but reduce the hydrogen absorption rate. Zhu et al. [17] investigated the cycle performance of $LaNi_{5-x}Co_x$ (x = 0, 0.25, 0.50 and 0.75) alloys. They found that the addition of Co lowered the plateau pressure and increased the stability of the hydride. After 1000 cycles, the $LaNi_{4.5}Co_{0.5}$ alloy still maintains a better crystal structure, larger particle size, and higher cycle stability than the $LaNi_5$ alloy. Other researchers have also studied novel methods to optimize the hydrogen storage performance of $LaNi_5$, such as surface modification [18] and so on.

Mechanical alloying, a novel method of synthesizing materials, is a solid-state powder processing technique that involves repeated cold welding, fracture, and rewelding of powder particles in a high-energy ball mill [19]. As a new synthesis method different from the traditional smelting method, mechanical alloying has many unique advantages, such as simple equipment, low cost, and it is easy to produce nanocrystals and metastable phases [20]. Because of the easy formation of nanocrystals, mechanical alloying has been proven to be a very effective method to improve the hydrogen storage properties of alloys [21-24].

In this work, the first-principles-based simulation method was used to select the replacement elements of $LaNi_5$, followed by the combination of mechanical alloying and element substitution to optimize the hydrogen storage performance of $LaNi_5$.

2.Experimental methods

2.1 The first principle simulation method

The structure of $LaNi_5$ is shown in Fig. 1. Its unit cell belongs to the P6/mmm space group. The crystal system is hexagonal. The lattice parameters are a=b=0.495 nm, c=0.394 nm. Among them, 1 La atoms occupying La(1a) site, 5 Ni atoms occupy Ni(2c) and Ni(3g) sites, respectively. In order to study the case of element substitution, the Mn, Pd, Cu, Cr, Co, Sn, Zn and Fe atoms were introduced into the structure to substitute Ni atom. In this case, one Ni atom

was substituted. Substitution atoms were sequentially introduced into different positions of Ni, and the corresponding total energies were calculated. In this work, the formation enthalpy is defined as the difference between the total energy and the energy of the constituent elements in the steady state. The enthalpy of formation can be used to demonstrate whether a compound is thermodynamically superior to the constituent elements, and subsequently determine which positions are preferentially occupied by these elements. The enthalpy of formation is defined as following formula [25]:

$$E_F=E_{tot}(La_xNi_yX_z) - [xE(La) + yE(Ni) + zE(X)] \quad (1)$$

Where E_F is the enthalpy of formation of alloy. E_{tot} is the total energy. E is the energy of one atom. The X in formula is the substitution element.

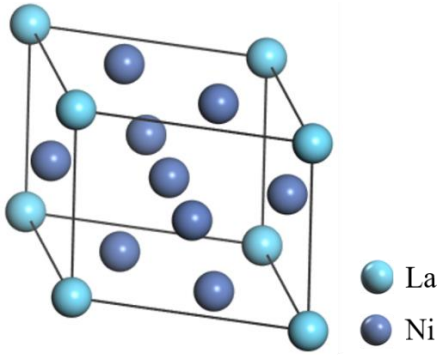

Fig. 1. The structure of $LaNi_5$

The calculation relied on the CASTEP programme, which is a first principles quantum mechanical code based on the density functional theory [26]. The Perdew–Burke–Ernzerhof (PBE) generalized gradient approximation (GGA) exchange and correlation potential were used in the calculations. In the calculation, ultrasoft pseudopotentials were used for replacing the core electrons. The energy cutoff is 380 eV and the k-point sets are 1×1×1 during all the process. Other parameters for geometry optimization are below: convergence criteria: 5.0×10^{-6} eV/atom, maximum force: 0.01 eV/Å, maximum stress: 0.02 GPa and maximum displacement: 5.0×10^{-4} ˚A. [27]

2.2 Mechanical alloying synthesis alloys

Mechanical alloying is a solid-state processing method whose mechanism involves repeated welding, fracture, and rewelding of powder particles in a high-energy ball mill [28]. The vial and the support plate rotate in opposite directions, and the centrifugal force acts alternately in the same direction and in the opposite direction. Two effects dominate this process, among which the friction effect occurs because the steel balls run along the inner wall of the container, and the impact effect occurs because the powder and steel balls rise up, pass through the inner chamber of the container and collide with the opposite inner wall collision.

Mechanical alloying can reduce the crystal size, introduce a large number of grain boundaries and defects, and promote the formation of nanostructures and amorphous phases. The reduction of the average size of the hydrogenated phase and the increase of the phase boundary volume fraction can lead to higher hydrogen absorption capacity and faster hydrogen absorption kinetics of hydrogen storage alloys [29], which is why mechanical alloying methods have been extensively studied.

In the initial stage of mechanical alloying, the powder is not like the alloys produced by melting and casting, in which the interatomic bonding between the components is fully achieved to form a uniform solid solution or compound. Instead, the components reach close to atomic-level distances at those points, lines and surfaces that are in contact, and what is obtained is only a very uniform mixture or compound of the components [30]. When the milling time is further extended, solid-state diffusion will occur in the system, so that the components can be bonded between atoms to form alloys or compounds. As the ball milling time prolongs, the input energy increases, and structural defects, such as lattice dislocation, interstitial sites and stresses increase, and eventually gaps are formed to make the phase brittle and the particles are easier to break. So, the grain size will go down and strain rate will increase as milling time goes up [31].

The PM400 model planetary ball mill of Retsch company was used to synthesis the alloys. Pure La, Ni and Cr were put into vessels according to chemical formulas. The ratio of ball to powder is 1:10. The speed is 400 rpm, and the time of milling time was set as 20h, 30h, 40h and 50h to select the optimal one. After screening by XRD and PCT tests, we chose to use the parameters of 40h mechanical alloying to synthesize Cr-doped 40h milled $LaNi_5$. Its chemical formula is $LaNi_4Cr$.

2.3 X-ray diffraction measurements

In the current study, XRD was performed on a Bruker D8 Advance X-ray diffractometer with Cu Kα radiation ($\lambda = 0.15418$ nm) filtered by nickel. Meanwhile, the grain size and strain of all the samples were also calculated. The calculation method and principle are listed below. Sometimes, we can find that the diffraction peaks are wider than the conventional ones. The first reason is that the crystal grains of the samples are smaller than those of conventional samples, resulting in a larger reciprocal sphere, which broadens the diffraction peaks. Another reason is that various processing methods can generate microscopic strains inside the grains. If there are two situations in the sample at the same time, use the Hall method [32], that is, measure the FWHM(Full width at half maximum) of more than two diffraction peaks, and then take $\sin(\theta)/\lambda$ as the abscissa, and make $FWHM*\cos(\theta)/\lambda-\sin(\theta)/\lambda$ diagram, using the least squares method for straight line fitting, the slope of the straight line is twice the microscopic strain, and the intercept of the straight line is the reciprocal of the grain size. All the above operations were carried out in the software JADE. We also bought $LaNi_5$ powder from SIGMA-ALDRICH company, and set it as the standard melting-produced sample.

2.4 Pressure-Composition-Temperature (PCT) tests

The PCT-Pro equipment of SERARAM company was applied for the PCT test, which shown in Fig.2. After synthesizing, the powder was load into the sample holder. Before the PCT, the alloys were subjected to four hydrogen absorption/desorption cycles in a 60 bar hydrogen atmosphere at 100 °C to activate and the example activation graph was shown in Fig.3. The ΔP was set to 60 bar, the Δt for absorption was 120 min and for absorption was 20 min. After, the PCT proceeds. The working principle of the PCT equipment is shown in Fig.4. In the first stage, the hydrogen stage will increase from 0 to ΔP. During this stage, alloys will start to absorb

hydrogen, so the hydrogen pressure will decrease slightly. The absorption will stop when the time reaches to Δt or the absorption rate reaches to the rate limitation. Then, the pressure will increase from ΔP to 2ΔP, and absorption starts again. All the mentioned procedures will repeat and repeat until the pressure reaches to the pressure limit. When all the absorption finishes, the software will link all the points which are located on the end of every absorption stage, which means the overall PCT curve is produced (red line in the Fig.4). The parameters of PCT are listed below: ΔP=2 bar, Δt= 60 min, rate limit= 0.01 wt.%/min, pressure limit= 8 bar.

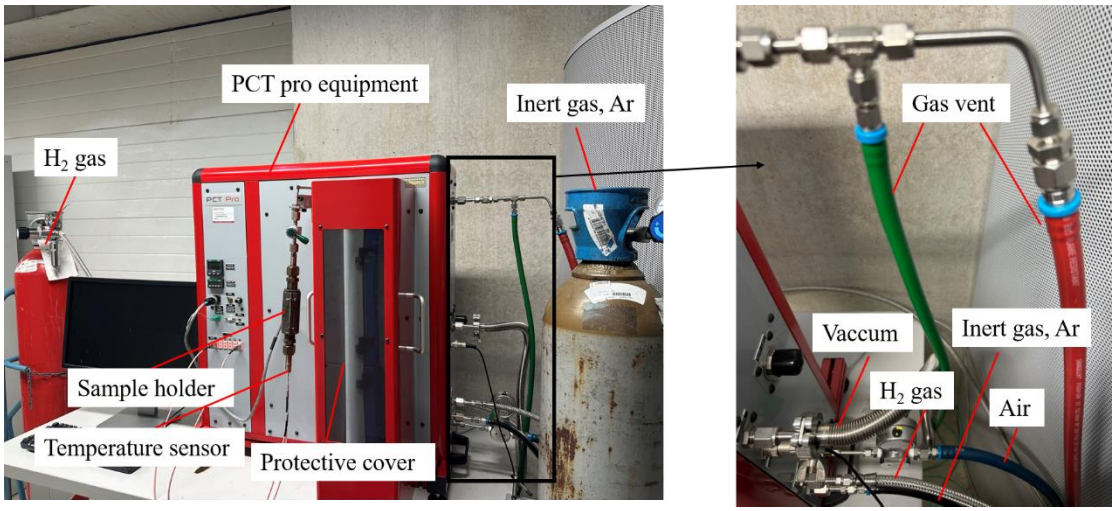

Fig.2 PCT-Pro equipment of SERARAM company

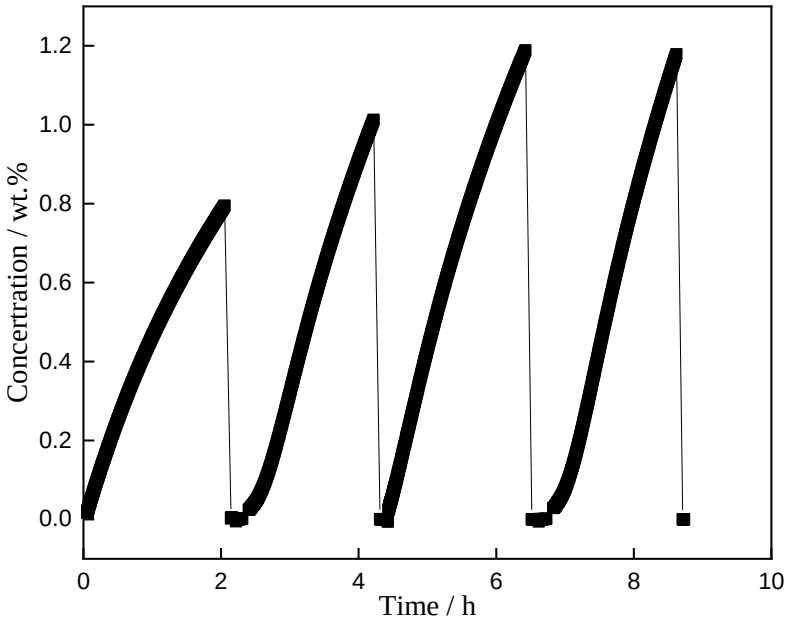

Fig.3 The example graph of activation before PCT (100 ℃, H_2 60 bar).

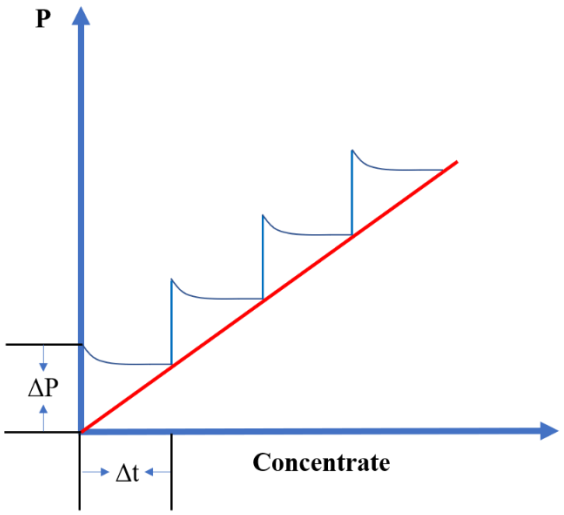

Fig.4 Schematic diagram of PCT equipment performing PCT test

2.5 Electrochemical tests

In this study, the SP-50 model electrochemical workstation of BioLogic company was applied for the electrochemical test. Measurements were made using a three-electrode system. The working electrode is composed of wire, Ni mesh and powder sample. The powder sample is an alloy powder, and carbon black and PTFE(Polytetrafluoroethylene) are mixed in a certain proportion. Platinum sheet and Hg/HgO were respectively employed as counter electrode and reference electrode. The applied current is calculated according to the proportion of alloy powder in the sample. The cut-off voltage for charging is -1.3V, and the cut-off voltage for discharging is -0.6V. The electrolyte was 6 M KOH aqueous solution. In order to eliminate adverse oxidative effects, the electrodes were soaked in the electrolyte 24h at room temperature and 1h at 100°C for activation, before electrochemical tests of each sample.

3.Results and discussion

3.1 Selection of substitution element by first principles simulation

The calculation of the enthalpy of formation which shown in Fig. 5 was carried out with the method mentioned above. The conclusion that we can extract from this figure are: First, as substitution atoms enter the unit cell, the enthalpy of formation of all alloys reduce, which means the reduction of phase stability. Second, Mn, Cr, Co and Fe have the higher enthalpy of formation compared to other four elements. And third, among the elements we selected, Cr has the highest enthalpy of formation. Actually, after the doping elements are introduced into the alloy, due to the difference in the volume of the doping atoms and the in-situ atoms, the volume of the surrounding tetrahedral interstitial and octahedral interstitial will accordingly change, which also induced the change in phase stability [33][34]. So, the change of the maximum discharge capacity is caused by the change of the phase stability due to the entry of doping elements. Compared with the original alloy, the enthalpy of formation of the substituted alloy decreases less, indicating that the phase stability decreases less, which is equivalent to the smaller the change of the lattice, so the hydrogen storage capacity decreases less. Based on this

idea, we choose Cr as the substitution element.

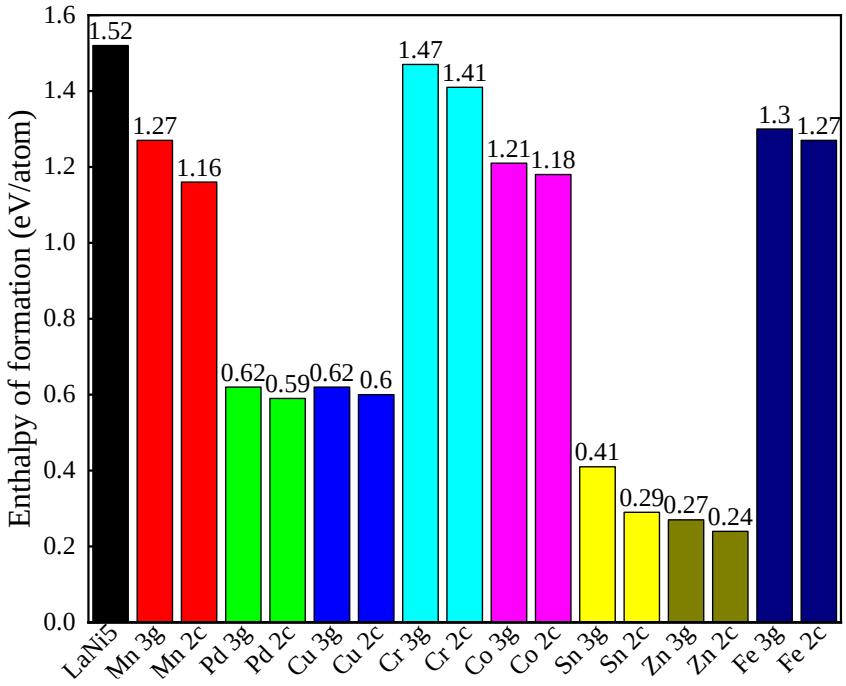

Fig.5 The results of simulation

3.2 The microstructure characterization of the different alloys

The X-ray diffraction results are shown in Fig.6.

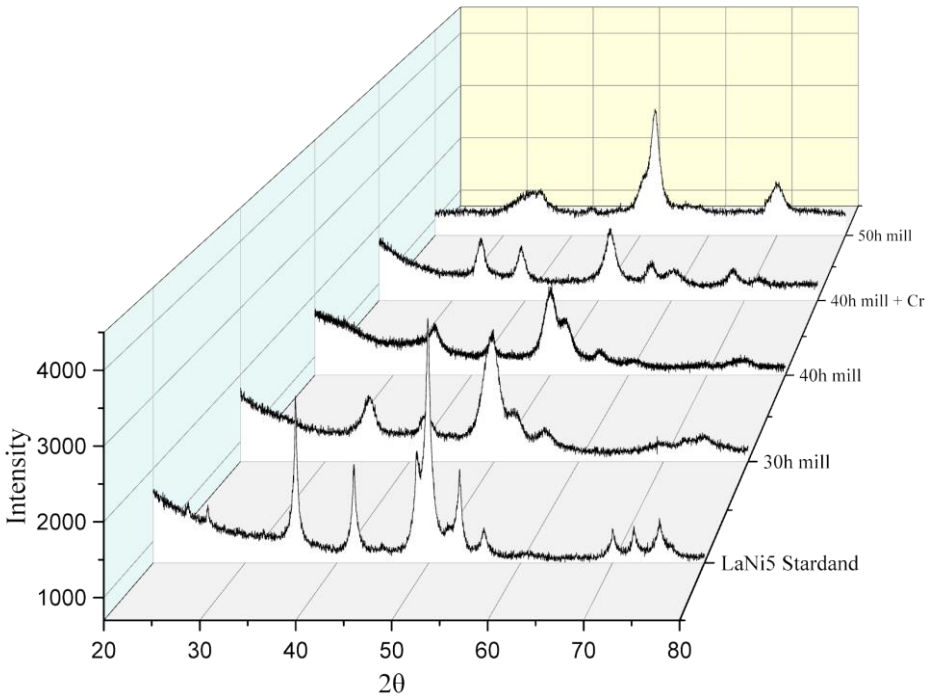

Fig.6 X-Ray diffraction of the different alloys

As shown in Fig.6, we set the XRD of standard $LaNi_5$ as the standard graph. The peak positions of all the milled sample are almost same compared to the standard one, so we can say we successfully synthesis the $LaNi_5$. From XRD graphs, some conclusions reveal. First, compared

to standard graph, the XRD peak intensity of all mill samples decreased and the width increased. This means that the grain size of the ball-milled samples is drastically reduced compared to the standard smelted samples [35]. Second, compared to other milled samples, 50h milled sample has the largest peak width. It can be seen that at many positions, such as 2θ=30 or 70, its peak is equivalent to several peaks of other samples combined together. This shows that in the 50h milled sample, most of the grains have become amorphous. Such alloys are no longer suitable for hydrogen storage. So in the following tests and calculations, only 30h milled sample, 40h milled sample are included.

As mentioned in experiment methods part, the mechanical alloying will cause the decrease of grain size and the increase of strain rate. These two values can be calculated according to the XRD with Hall method. The results of calculation of grain size and strain rate are shown in Table.1, which is consistent with the conclusion above.

Table.1 Grain size and stain rate results of the samples according to XRD

alloy	Grain size (nm)	Strain rate
standard $LaNi_5$	313 ± 3	0.142%
30h milled $LaNi_5$	43 ± 1	1.589%
40h milled $LaNi_5$	39 ±2	2.064%
40h milled $LaNi_4Cr$	53 ±1	0.863%

3.3 PCT test results

The PCT test was performed after activation and the results of the test are shown in Fig.7. A series of conclusions can be extracted from the results.

First, as Fig.7 (a) shows, it can be found that the capacity and equilibrium pressure of standard $LaNi_5$ are much worse than those of 40h milled $LaNi_5$. This can be interpreted by the difference of grain size and strain. According to the Table.1, the grain size of melted sample is 313 nm, and that of milled one is about 40-60 nm, and the strain of milled samples is much more than melted sample. Larger microstrains mean more defects. The nanocrystalline microstructure produced by ball milling provides a large number of defects and grain boundaries near the powder surface. This greatly reduces the energy required for hydrogenation. The energy required is intuitively expressed as the equilibrium pressure, the lower the equilibrium pressure, the lower the energy required for the reaction. Thus, milled samples have the lower equilibrium pressure. Other researchers have expressed the same view [36][37], that is, small grains and large strains can reduce the energy required for hydrogenation. At the same time, defects such as dislocations and grain boundaries can increase the sites for hydrogen to reside [38], which is equivalent to improving the hydrogen storage capacity.

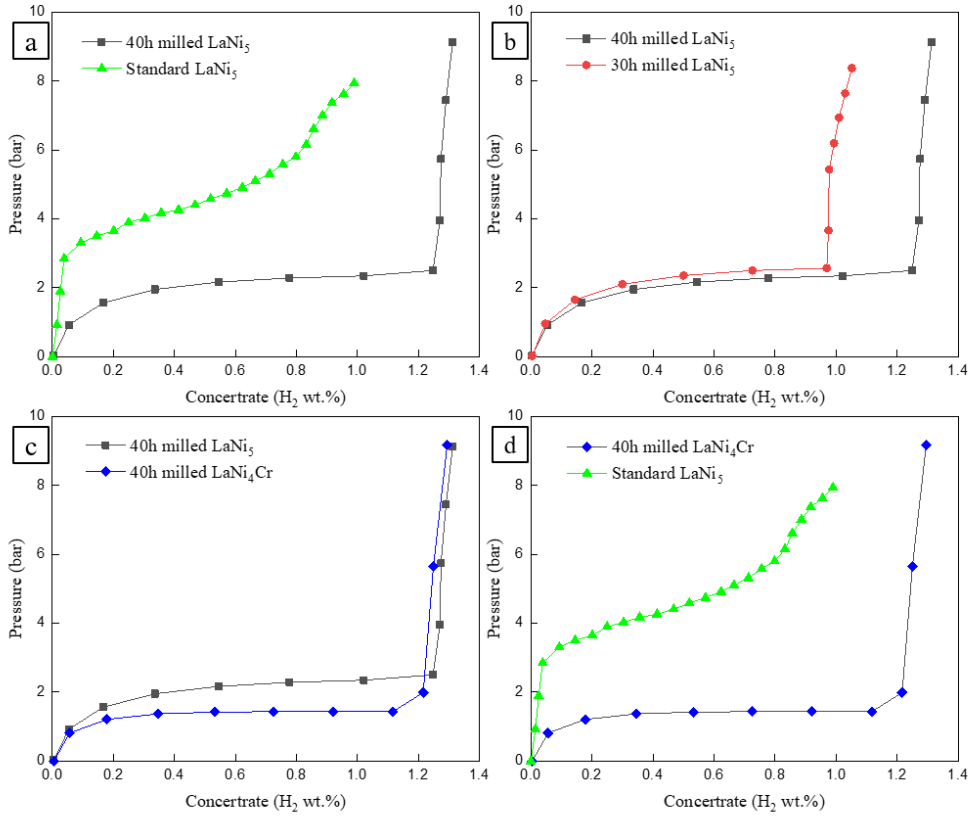

Fig.7. The PCT curves of the different alloys

Second, from the as Fig.7 (b) which focus on the PCT of 40h milled $LaNi_5$ and 30h milled $LaNi_5$, we can conclude the influence of the milling time. The most obvious difference is the change in capacity. According to the XRD results, the strain rate of 40h milled sample is much higher than that of 30h milled sample. As listed above, the increase of hydrogen storage capacity is contributed to the increase in the number of defects brought by strains. In the enlarged view of the PCT diagram, it can also be observed that the kinetic of the 40h milled sample is slightly better than that of the 30h milled sample. This can be explained by the increased surface area due to the reduced grain size. The smaller grain size, the larger surface area. The large surface area means that when the particles react with hydrogen, the number of hydrogen molecules in contact with them at the same time will increase. In the case that the surface reaction rate is not affected, this means that the reaction rate is improved. Moreover, the exposure of fresh surfaces by ball milling, which tend to have more defects, reduces the energy required for hydrogen to attach to the grain surface, which further increases the reaction rate. Yahui Sun, et al. [39] indicated that as the surface area of nanomaterials increases, more atoms are exposed on the surface, resulting in an increase in surface energy, which will result in lower enthalpy. L Guoxian, et al. [40] found the induced lattice defects can assist the diffusion of hydrogen in materials by providing many sites with low activation energy for diffusion.

Third, the Fig.7 (c) compares the PCT curves of 40h milled sample and 40h milled $LaNi_4Cr$, it can be found that the hydrogen storage capacity of the former is higher than that of the latter, but the equilibrium pressure of the latter is lower than the former. This is mainly related to the doping of Cr. According to XRD, the doping of Cr did not form a new phase. Zhang Y et al.

[41] believe that Cr is pinned on the grain boundary, and during quenching, Cr will prevent the movement of the grain boundary, thereby making the grain size smaller. However, in the process of mechanical alloying, if the movement of the grain boundaries is hindered, the process of reducing the size of the grains will be hindered, so that the final grain size will increase compared with that of the undoped alloy. The movement of grain boundaries is hindered, and at the same time, the number of internal defects in alloy grains is reduced, and the internal stress is reduced. This conclusion can be confirmed by the calculation results of XRD. The reduction in the number of defects leads to a reduction in the number of additional hydrogen sites, which can explain the reduction in the hydrogen storage capacity of the doped samples. Devendra Vyas et al. [42] found that the entry of Cr into the lattice can significantly reduce the stability of hydrides. This means that less energy is required to form the hydride. As mentioned above, the equilibrium pressure is directly related to the energy required to form the hydride. Although the entry of Cr reduces the degree of lattice lowering and reduces the strain in the lattice, $LaNi_4Cr$ has a lower equilibrium pressure and better kinetics due to the catalytic effect of Cr on hydride formation.

Fourth, the Fig.7 (d) shows the overall influence of combination of mechanical alloying and substitution. It can be seen that after the optimization, the capacity and kinetics of $LaNi_5$ improve dramatically. Mechanical alloying externally changes the alloy. This method reduces the particle size and introduces a large number of defects, providing more opportunities for hydrogen to contact the alloy surface and more accommodation sites. At the same time, element substitution changes the alloy internally. The substitution atom replaces the atoms in the original crystal lattice, causing the change of size of the crystal lattice. Futhermore, the substitution elements themselves will optimize the properties of the alloy. Combining the above factors, the hydrogen storage performance of $LaNi_5$ has been greatly optimized.

3.4 Electrochemical test results

Electrochemical tests were carried out to characterize the electrochemical properties of milled samples. The results are shown in Fig.8 and the data extracted from the graph are listed in the Table.2 It can be found that the maximum discharge capacity of 30h milled $LaNi_5$ and 40h milled $LaNi_4Cr$ are less than that of 40h milled $LaNi_5$, this is consistent with the results of PCT. We can find the cycle stability of 30h milled $LaNi_5$ is worse than that of 40h milled $LaNi_5$. The decline in the maximum discharge capacity of the hydrogen storage alloy is mainly due to the repeated expansion and contraction of the crystal lattice during the cycle of hydrogen absorption and desorption, which leads to the gradual deterioration of the alloy structure and even pulverization [43]. The internal strain of 40h milled $LaNi_5$ is larger, so there are more defects in the grain. A lattice with a high number of defects is more tolerant of lattice expansion or contraction. When the lattice structure with few defects is gradually destroyed by hydrogen absorption expansion or hydrogen desorption contraction, the lattice with many defects can use these defects to offset part of the structural changes, so that its cycle stability increases [44].

On the contrary, the cycle stability of 40h milled $LaNi_4Cr$ is much better than that of 40h milled $LaNi_5$. As mentioned above, Cr pins on grain boundaries and prevents grain boundary movement. And Cr has a catalytic effect on the formation of hydrides. Therefore, the samples containing Cr not only have high cycle stability, but also have not low maximum discharge capacity. Wang X et al. [45] also found that Cr leads to a decrease in the discharge capacity, but

the doping of Cr significantly improves the cycle stability of the alloy.

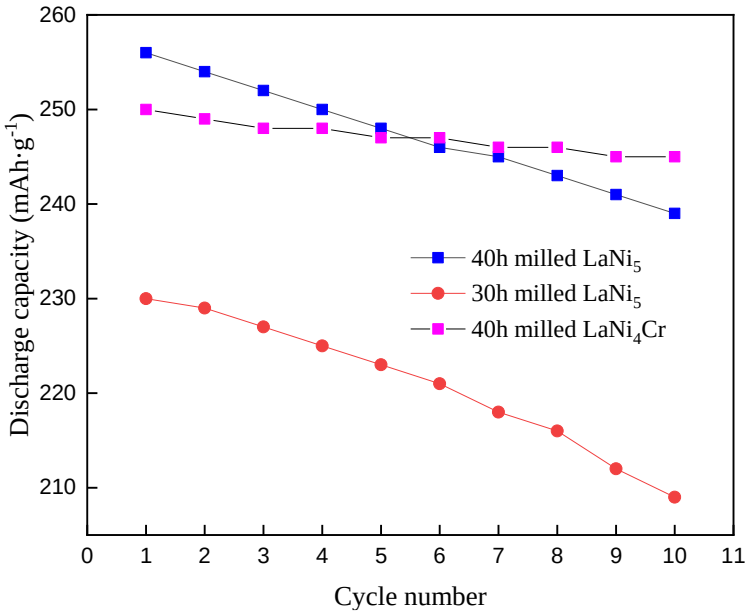

Fig.8 Discharge capacity of the different milled alloys

Table.2 The Maximum discharge capacity and Capacity retention after10 cycles of the different milled alloys

alloy	Maximum discharge capacity ($mAh \cdot g^{-1}$)	Capacity retention after 10 cycles
30h milled $LaNi_5$	230	91.23%
40h milled $LaNi_5$	256	94.73%
40h milled $LaNi_4Cr$	250	99.2%

4. Conclusion

In this work, simulation based on the first principle was applied to predict the performance of $LaNi_5$ after elements substituting Ni. One Mn, Pd, Cu, Cr, Co, Sn, Zn or Fe was induced to replace one Ni atom, and the enthalpy of formation was calculated.

The results show that, the enthalpy of formation of all alloys reduce when substitution atom go into the unit cell, and Cr has the highest enthalpy of formation. So, Cr was selected to substitute Ni in $LaNi_5$. After, the X-Ray Diffraction was applied to characterize the phase composition, Pressure-Composition-Temperature (PCT) curves and electrochemical technique were used to test the hydrogen properties. It was revealed that, $LaNi_5$ with different milling time was successfully synthesized, including 40h milled $LaNi_4Cr$. The mechanical alloying can improve the capacity, kinetics and reduce the plateau pressure due to the small grain size and large internal strain. Compared with 30h and 50h, 40h is a more suitable milling time. And for the Cr substitution, the hydrogen storage performance of $LaNi_5$ is further enhanced due to the combination of mechanical alloying and Cr pinning on grain boundaries. The gaseous hydrogen storage capacity of 40h milled $LaNi_4Cr$ reaches 1.13 wt.%, the plateau pressure goes to 1.1bar. The results of electrochemical test showed that the maximum discharge capacity is about 250 $mAh \cdot g^{-1}$, and the capacity retention after 10 cycles is 99.2%. In summary, the combination of

mechanical alloying and element substitution can greatly optimize the hydrogen storage performance of LaNi5 alloy.

Acknowledgement

The work was supported by China Scholarship Council (China) and UTBM (France) in the framework of UT-INSA project (2020).

References

[1] Salehabadi A, Dawi E A, Sabur D A, et al. Progress on nano-scaled alloys and mixed metal oxides in solid-state hydrogen storage; an overview[J]. Journal of Energy Storage, 2023, 61: 106722. https://doi.org/10.1016/j.est.2023.106722

[2] Kumar A, Muthukumar P, Sharma P, et al. Absorption based solid state hydrogen storage system: A review[J]. Sustainable Energy Technologies and Assessments, 2022, 52: 102204. https://doi.org/10.1016/j.seta.2022.102204

[3] Simanullang M, Prost L. Nanomaterials for on-board solid-state hydrogen storage applications[J]. International Journal of Hydrogen Energy, 2022, 47(69): 29808-29846. https://doi.org/10.1016/j.ijhydene.2022.06.301

[4] Li Q, Lin X, Luo Q, et al. Kinetics of the hydrogen absorption and desorption processes of hydrogen storage alloys: A review[J]. International Journal of Minerals, Metallurgy and Materials, 2022, 29: 32-48. https://doi.org/10.1007/s12613-021-2337-8

[5] Zhang Y, Li C, Yuan Z, et al. Research progress of TiFe-based hydrogen storage alloys[J]. Journal of Iron and Steel Research International, 2022, 29(4): 537-551. https://doi.org/10.1007/s42243-022-00756-w

[6] Sui Y, Yuan Z, Zhou D, et al. Recent progress of nanotechnology in enhancing hydrogen storage performance of magnesium-based materials: A review[J]. International Journal of Hydrogen Energy, 2022, 47(71): 30546-30566. https://doi.org/10.1016/j.ijhydene.2022.06.310

[7] Wu R, Yuan H, Luo Q, et al. Carbon coating with different carbon sources on rare earth hydrogen storage alloy[J]. International Journal of Hydrogen Energy, 2023. https://doi.org/10.1016/j.ijhydene.2023.04.282

[8] Ding N, Liu D, Liu W, et al. Excellent kinetics and effective hydrogen storage capacity at low temperature of superlattice rare-earth hydrogen storage alloy by solid-phase treatment[J]. Journal of Physics and Chemistry of Solids, 2022, 161: 110402. https://doi.org/10.1016/j.jpcs.2021.110402

[9] Jiang W, Chen Y, Hu M, et al. Rare earth-Mg-Ni-based alloys with superlattice structure for electrochemical hydrogen storage[J]. Journal of Alloys and Compounds, 2021, 887: 161381. https://doi.org/10.1016/j.jallcom.2021.161381

[10] Sakai T, Yoshinaga H, Miyamura H, et al. Rechargeable hydrogen batteries using rare-earth-based hydrogen storage alloys[J]. Journal of alloys and compounds, 1992, 180(1-2): 37-54. https://doi.org/10.1016/0925-8388(92)90361-C

[11] Nahm K S, Kim W Y, Hong S P, et al. The reaction kinetics of hydrogen storage in LaNi5[J]. International Journal of Hydrogen Energy, 1992, 17(5): 333-338. https://doi.org/10.1016/0360-

3199(92)90169-W
[12] Sakai T, Miyamura H, Kuriyama N, et al. Metal hydride anodes for nickel-hydrogen secondary battery[J]. Journal of the Electrochemical Society, 1990, 137(3): 795. https://doi.org/10.1149/1.2086557
[13] Hassan I A, Ramadan H S, Saleh M A, et al. Hydrogen storage technologies for stationary and mobile applications: Review, analysis and perspectives[J]. Renewable and Sustainable Energy Reviews, 2021, 149: 111311. https://doi.org/10.1016/j.rser.2021.111311
[14] Joubert J M, Paul-Boncour V, Cuevas F, et al. LaNi5 related AB5 compounds: Structure, properties and applications[J]. Journal of Alloys and Compounds, 2021, 862: 158163. https://doi.org/10.1016/j.jallcom.2020.158163
[15] Todorova S, Abrashev B, Rangelova V, et al. Hydrogen gas phase and electrochemical hydriding of LaNi5− xMx (M= Sn, Co, Al) alloys[J]. Materials, 2020, 14(1): 14. https://dx.doi.org /10.3390/ma14010014
[16] Somo T R, Modibane K D, Davids M W, et al. Improvement of hydriding kinetics of LaNi 5-type metal alloy through substitution of nickel with tin followed by palladium deposition[J]. Bulletin of Materials Science, 2022, 45: 1-11. https://doi.org/10.1007/s12034-021-02591-3
[17] Zhu Z, Zhu S, Lu H, et al. Stability of LaNi5-xCox alloys cycled in hydrogen—Part 1 evolution in gaseous hydrogen storage performance[J]. international journal of hydrogen energy, 2019, 44(29): 15159-15172. https://doi.org/10.1016/j.ijhydene.2019.04.111
[18] Li K, Huang T, Gao Y, et al. Enhancing antioxidant properties of hydrogen storage alloys using PMMA coating[J]. International Journal of Hydrogen Energy, 2023, 48(11): 4339-4348. https://doi.org/10.1016/j.ijhydene.2022.10.208
[19] Suryanarayana C. Mechanical alloying: a novel technique to synthesize advanced materials[J]. Research, 2019, 2019: 4219812. https://doi.org/10.34133/2019/4219812
[20] Shuai C, He C, Peng S, et al. Mechanical alloying of immiscible metallic systems: process, microstructure, and mechanism[J]. Advanced Engineering Materials, 2021, 23(4): 2001098. https://doi.org/10.1002/adem.202001098
[21] Küçükdeveci N, Erdoğan I A, Aybar A B, et al. Electrochemical hydrogen storage properties of mechanically alloyed Mg0. 8Ti0. 2-xMnxNi (x= 0, 0.025, 0.05, 0.1) type alloys[J]. International Journal of Hydrogen Energy, 2022, 47(4): 2511-2519. https://doi.org/10.1016/j.ijhydene.2021.10.174
[22] Shahi R R, Gupta A K, Kumari P. Perspectives of high entropy alloys as hydrogen storage materials[J]. International Journal of Hydrogen Energy, 2023, 48(56): 21412-21428. https://doi.org/10.1016/j.ijhydene.2022.02.113
[23] Suryanarayana C, Al-Joubori A A, Wang Z. Nanostructured materials and nanocomposites by mechanical alloying: an overview[J]. Metals and Materials International, 2022, 28(1): 41-53. https://doi.org/10.1007/s12540-021-00998-5
[24] Liu Y, Chabane D, Elkedim O. Intermetallic compounds synthesized by mechanical alloying for solid-state hydrogen storage: A review[J]. Energies, 2021, 14(18): 5758. https://doi.org/10.3390/en14185758
[25] Huang L W, Elkedim O, Hamzaoui R. First principles investigation of the substitutional doping of Mn in Mg2Ni phase and the electronic structure of Mg3MnNi2 phase[J]. Journal of Alloys and Compounds, 2011, 509: S328-S333. https://doi.org/10.1016/j.jallcom.2010.08.129
[26] Clark S J, Segall M D, Pickard C J, et al. First principles methods using CASTEP[J].

Zeitschrift für kristallographie-crystalline materials, 2005, 220(5-6): 567-570. https://doi.org/10.1524/zkri.220.5.567.65075
[27] Liu Y, Chabane D, Elkedim O. First principles investigation of the substitutional doping of rare-earth elements and Co in La4MgNi19 phase[J]. Journal of Energy Storage, 2023, 67: 107638. https://doi.org/10.1016/j.est.2023.107638
[28] Suryanarayana C. Mechanical alloying and milling[J]. Progress in materials science, 2001, 46(1-2): 1-184. https://doi.org/10.1016/S0079-6425(99)00010-9
[29] Yim C D, You B S, Na Y S, et al. Hydriding properties of Mg–xNi alloys with different microstructures[J]. Catalysis Today, 2007, 120(3-4): 276-280. https ://doi.org/10.1016/j.cattod.2006.09.020
[30] Michalchuk A A L, Boldyreva E V, Belenguer A M, et al. Tribochemistry, mechanical alloying, mechanochemistry: what is in a name?[J]. Frontiers in chemistry, 2021, 9: 685789. https://doi.org/10.3389/fchem.2021.685789
[31] Vaidya M, Muralikrishna G M, Murty B S. High-entropy alloys by mechanical alloying: A review[J]. Journal of Materials Research, 2019, 34(5): 664-686. https://doi.org/10.1557/jmr.2019.37
[32] Bakshi S D, Sinha D, Chowdhury S G. Anisotropic broadening of XRD peaks of α′-Fe: Williamson-Hall and Warren-Averbach analysis using full width at half maximum (FWHM) and integral breadth (IB)[J]. Materials Characterization, 2018, 142: 144-153. https://doi.org/10.1016/j.matchar.2018.05.018
[33] Liu Y, Yuan H, Guo M, et al. Effect of Y element on cyclic stability of A2B7-type La–Y–Ni-based hydrogen storage alloy[J]. International Journal of Hydrogen Energy, 2019, 44(39): 22064-22073. https://doi.org/10.1016/j.ijhydene.2019.06.081
[34] Liu J, Li Y, Han D, et al. Electrochemical performance and capacity degradation mechanism of single-phase La–Mg–Ni-based hydrogen storage alloys[J]. Journal of Power Sources, 2015, 300: 77-86. https://doi.org/10.1016/j.jpowsour.2015.09.058
[35]Chauhan A, Chauhan P. Powder XRD technique and its applications in science and technology[J]. J Anal Bioanal Tech, 2014, 5(5): 1-5. https://doi.org/10.4172/2155-9872.1000212
[36] Garara M, Benzidi H, Abdellaoui M, et al. Hydrogen storage properties of perovskite-type $MgCoH_3$ under strain effect[J]. Materials Chemistry and Physics, 2020, 254: 123417. https://doi.org/10.1016/j.matchemphys.2020.123417
[37] Zaluska A, Zaluski L, Ström–Olsen J O. Nanocrystalline magnesium for hydrogen storage[J]. Journal of Alloys and Compounds, 1999, 288(1-2): 217-225. https://doi.org/10.1016/S0925-8388(99)00073-0
[38] Revesz A, Gajdics M. Correlation between microstructure and hydrogen storage properties of nanocrystalline magnesium subjected to high-pressure torsion[C]//Materials Science Forum. Trans Tech Publications Ltd, 2017, 885: 67-73. https://doi.org/10.4028/www.scientific.net /MSF.885.67
[39] Sun Y, Shen C, Lai Q, et al. Tailoring magnesium based materials for hydrogen storage through synthesis: Current state of the art[J]. Energy Storage Materials, 2018, 10: 168-198. https://doi.org/10.1016/j.ensm.2017.01.010
[40] Guoxian L, Erde W, Shoushi F. Hydrogen absorption and desorption characteristics of mechanically milled Mg□ 35wt.% FeTi1. 2 powders[J]. Journal of Alloys and Compounds,

1995, 223(1): 111-114. https://doi.org/10.1016/0925-8388(94)01465-5
[41] Zhang Y, Li B, Ren H, et al. Effects of Cr addition on the microstructures and electrochemical properties of as-cast and quenched La2Mg (Ni0. 85Co0. 15) 9 electrode alloys[J]. Journal of alloys and compounds, 2007, 436(1-2): 209-215. https://doi.org/10.1016/j.jallcom.2006.07.006
[42] Vyas D, Jain P, Agarwal G, et al. Hydrogen storage properties of Mg2Ni affected by Cr catalyst[J]. international journal of hydrogen energy, 2012, 37(21): 16013-16017. https://doi.org/10.1016/j.ijhydene.2012.08.039
[43] Liu J, Li Y, Han D, et al. Electrochemical performance and capacity degradation mechanism of single-phase La–Mg–Ni-based hydrogen storage alloys[J]. Journal of Power Sources, 2015, 300: 77-86. https://doi.org/10.1016/j.jpowsour.2015.09.058
[44] Peisl H. Lattice strains due to hydrogen in metals[J]. Hydrogen in metals I: Basic properties, 2005: 53-74. https://doi.org/10.1007/3540087052_42
[45] Wang X, Zhang Y, Zhao D, et al. Effects of Cr addition on the microstructures and electrochemical performances of La–Mg–Ni system (PuNi3-type) hydrogen storage alloy[J]. Journal of alloys and compounds, 2007, 446: 625-629. https://doi.org/10.1016/j.jallcom.2007.01.062